

ORIGINAL RESEARCH

Vitamin D Receptor Activation Targets ROS-Mediated Crosstalk Between Autophagy and Apoptosis in Hepatocytes in Cholestatic Mice

Zhijian Zheng,¹ Jing Xie,² Liman Ma,² Zhiqing Hao,³ Weiwei Zhang,³ and Lihua Li¹

¹Department of General Surgery, Affiliated Wenling First People's Hospital, Taizhou University, Taizhou, Zhejiang Province, P R China; ²Department of Cell Biology, School of Medicine, Taizhou University, Taizhou, Zhejiang Province, P R China; ³Department of Pathophysiology, School of Basic Medicine, Shenyang Medical College, Shenyang, Liaoning Province, PR China

SUMMARY

Vitamin D receptor (VDR) agonist paricalcitol up-regulates VDR expression in hepatocytes in mice liver. Treatment with paricalcitol improves bile duct-ligated mice liver injury by reducing hepatocyte apoptosis. Up-regulation of VDR-inhibited apoptosis is autophagy-dependent and via the inhibiting reactive oxygen species generation by extracellular signal-regulated kinase/p38 mitogen-activated protein kinase pathway.

BACKGROUND & AIMS: Observational epidemiologic studies have associated vitamin D deficiency with cholestasis. We reported previously that activation of the vitamin D/vitamin D receptor (VDR) axis in cholangiocytes mitigates cholestatic liver injury by remodeling the damaged bile duct. However, the function of VDR in hepatocytes during cholestasis remains unclear.

METHODS: Paricalcitol (VDR agonist, 200 ng/kg) was injected intraperitoneally into bile duct-ligated mice every other day for 5 days. Primary hepatocytes and HepG2 hepatoma cells were transfected with *Vdr* short hairpin RNA, control short hairpin RNA, *Vdr* plasmid, control vector, *Atg5* small interfering RNA (siRNA), and control siRNA. Liver histology, cell proliferation, and autophagy were evaluated.

RESULTS: Treatment with the VDR agonist paricalcitol improved liver injury in bile duct-ligated mice by up-regulating VDR expression in hepatocytes, which in turn reduced hepatocyte apoptosis by inhibiting reactive oxygen species (ROS) generation via suppressing the Ras-related C3 botulinum toxin substrate 1/reduced nicotinamide adenine dinucleotide phosphate oxidase 1 pathway. Mechanistically, upon exposure to an ROS-inducing compound, *Vdr* siRNA contributed to apoptosis, whereas the *Vdr* overexpression caused resistance to apoptosis. Interestingly, up-regulated VDR expression also increased the generation of autophagosomes and macroautophagic/autophagic flux, which was the underlying mechanism for reduced apoptosis following VDR activation. Autophagy depletion impaired the positive effects of VDR overexpression, whereas autophagy induction was synergistic with VDR overexpression. Importantly, up-regulation of VDR promoted autophagy activation by suppressing the activation of the extracellular signal-regulated kinase (ERK)/p38 mitogen-activated protein kinase (p38MAPK) pathway. Thus, a p38MAPK inhibitor abrogated the

Vdr siRNA-induced decrease in autophagy and the *Vdr* siRNA-induced increase in apoptosis. In contrast, a Mitogen-activated protein kinase kinase (MEK)/ERK activator prevented the enhancement of autophagy and decreased apoptosis following *Vdr* overexpression. Moreover, the ROS inhibitor N-acetylcystein (NAC) blocked *Vdr* siRNA-enhanced activation of the ERK/p38MAPK pathway.

CONCLUSIONS: VDR activation mitigated liver cholestatic injury by reducing autophagy-dependent hepatocyte apoptosis and suppressing the activation of the ROS-dependent ERK/p38MAPK pathway. Thus, VDR activation may be a potential target for the treatment of cholestatic liver disease. (*Cell Mol Gastroenterol Hepatol* 2023;15:887–901; <https://doi.org/10.1016/j.jcmgh.2022.10.011>)

Keywords: Vitamin D-Receptor Activation; Autophagy; Apoptosis; ROS Generation; ERK/p38MAPK Pathway.

Cholestasis is a pathophysiological process of bile secretion and excretion disorders caused by viruses, alcohol, drugs, or immunity that can impair liver function, leading to liver fibrosis and liver cirrhosis and, ultimately, liver cancer, resulting in increased mortality.^{1,2} Recently, studies have shown that autophagy and apoptosis are involved in the occurrence and development of cholestatic liver injury, and autophagy is actually impaired in cholestasis, as shown by the increased accumulation of

Abbreviations used in this paper: ALT, alanine aminotransferase; AO, acridine orange; BDL, bile duct-ligated; BSA, bovine serum albumin; DHE, dihydroethidium; DMEM, Dulbecco's modified Eagle medium; ERK, extracellular signal-regulated kinase; MAPK, mitogen-activated protein kinase; MEK, Mitogen-activated protein kinase kinase; MMP, mitochondrial membrane potential; NOX, reduced nicotinamide adenine dinucleotide phosphate oxidase; OS, oxidative stress; PAL, paricalcitol; PBS, phosphate-buffered saline; PCR, polymerase chain reaction; PFA, paraformaldehyde; Rac1, Ras-related C3 botulinum toxin substrate 1; Rho123, rhodamine 123; ROS, reactive oxygen species; shRNA, short hairpin RNA; siRNA, small interfering RNA; SQSTM1, sequestosome 1; tBHP, *tert*-butyl hydroperoxide; TUNEL, terminal deoxynucleotidyl transferase-mediated deoxyuridine triphosphate nick-end labeling; VDR, vitamin D receptor.



Most current article

© 2023 The Authors. Published by Elsevier Inc. on behalf of the AGA Institute. This is an open access article under the CC BY-NC-ND license (<http://creativecommons.org/licenses/by-nc-nd/4.0/>).

2352-345X

<https://doi.org/10.1016/j.jcmgh.2022.10.011>

ubiquitinated proteins and autophagy substrate proteins found in bile duct-ligated (BDL) mice.^{3,4} Activation of autophagy eliminates the accumulation of reactive oxygen species (ROS) to alleviate cholestatic liver injury in BDL mice and reduces hepatocyte apoptosis *in vitro*.⁵ Manipulating autophagy and apoptosis may represent a new strategy for the treatment of cholestatic liver disease.

Recently, increasing evidence has suggested that the vitamin D receptor (VDR), a member of the nuclear receptor superfamily, may represent a therapeutic target in cholestatic diseases.⁶ The vitamin D–VDR axis protects hepatocytes from cholestatic injury by inhibiting the expression of genes involved in bile acid metabolism and transport,⁷ while VDR knockout exacerbates cholestatic liver injury by impairing bile duct integrity in mice.⁸ Our previous study showed that the VDR–yes-associated protein axis promotes cholangiocyte proliferation and enhances adaptive bile duct remodeling, alleviating cholestatic liver injury in BDL mice.⁹ In addition, VDR also can play a biological role in regulating autophagy and apoptosis. VDR inhibits the nuclear factor- κ B pathway to promote autophagy and inhibit apoptosis, which reduces the lipopolysaccharide-induced inflammatory response in the abalone hepatopancreas.¹⁰ VDR activation reduces oxidative stress (OS), inhibits apoptosis, and improves autophagy dysfunction to alleviate ischemia–reperfusion–induced myocardial injury in mice.¹¹ However, whether VDR is involved in regulating autophagy and apoptosis during cholestasis is unclear.

OS plays an important role in the regulation of autophagy and apoptosis. A study reported that reducing ROS production effectively inhibited human L02 cell apoptosis, which was largely dependent on up-regulation of autophagy via activation of LC3 and Beclin1, thereby alleviating OS-induced liver injury.¹² Blocking ROS generation can reduce mitochondrial pathway-dependent cell apoptosis and increase autophagic flux, alleviating CCl₄-induced acute liver injury in BALB/c mice.¹³ Under OS, ROS are released in high amounts by cells. There is evidence that the reduced nicotinamide adenine dinucleotide phosphate oxidase (NOX) complex plays a role in ROS generation, and NOX1-mediated ROS generation is dependent on the activation of Ras-related C3 botulinum toxin substrate 1 (Rac1).¹⁴ Studies have shown that reducing the expression of Rac1 and NOX1 can reduce ROS generation, thereby alleviating bile duct ligation-induced liver injury in rats.¹⁵ In addition, ROS can stimulate the activation of extracellular signal-regulated kinase (ERK; p42/p44) and p38 mitogen-activated protein kinase (MAPK),¹⁶ whose activation inhibits autophagosome formation and autophagic flux in human prostate cancer cells while inducing apoptosis, thereby attenuating prostate cancer progression.¹⁷ Moreover, activation of ERK and MAPK also can promote cell apoptosis in the gut and liver, thereby aggravating cholestatic liver injury in rats.¹⁸ Down-regulation of Rac1/NOX1 inhibits ROS production, which attenuates mitochondrial depolarization by inhibiting activation of the ERK and p38MAPK signaling pathways and reduces vascular smooth muscle cell apoptosis, thereby slowing the development of atherosclerosis in rats.¹⁹ Studies have shown that the vitamin D/VDR axis blocks

the activation of p38MAPK and ERK and inhibits podocyte apoptosis to protect the kidney from diabetic damage in mice.²⁰ VDR activation also can suppress pancreatic β -cell apoptosis by reducing ROS production²¹ and limiting the development of heart failure by inhibiting Rac1 expression.²² However, the specific mechanism by which the activation of VDR in hepatocytes alleviates cholestatic liver injury remains unclear. The present study shows that treatment with the VDR agonist paricalcitol (PAL) improves BDL mouse liver injury by up-regulating VDR expression in hepatocytes, which in turn reduces hepatocyte apoptosis. Moreover, up-regulated VDR-inhibited apoptosis is autophagy-dependent and occurs through inhibiting ROS generation and activation of the ROS-dependent ERK/p38MAPK pathway. Therefore, our results point to new therapeutic approaches for cholestatic liver injury.

Results

VDR Activation of Hepatocytes Was Responsible for Mitigated Hepatic Damage in BDL Mice

It has been reported that VDR expression is low in hepatocytes.²³ However, our research and that of others have found that VDR activation mitigates bile duct ligation- and nonalcoholic steatohepatitis-induced liver injury.^{23,24} Because the proportion of hepatocytes is largest in the liver, VDR expression in hepatocytes may be responsible for protecting the liver from injury. To investigate if PAL has a role in activation of VDR expression in hepatocytes of BDL mice liver, PAL was administered to mice following our previously reported protocol.⁹ Figure 1A shows the chemical structural formula of PAL. Hepatocytes were isolated from sham and BDL mouse livers at 5 days. Western blot and messenger RNA analysis showed that VDR expression was lower in both sham and BDL mice, but PAL greatly increased VDR expression ($P < .05$ or $P < .01$) (Figure 1B and C). Moreover, immunohistochemistry staining showed that PAL significantly increased VDR expression in the nucleus of hepatocytes in BDL mice (Figure 1D). To further assess if the biological function of VDR was activated, the expression levels of its target genes, *Cyp24a1* and *Sult2a1*, were examined. BDL triggered a reduction in the expression levels of *Cyp24a1* and *Sult2a1*, and this reduction was reversed by PAL ($P < .05$ or $P < .01$) (Figure 1E). In addition, we also examined the effect of PAL on VDR target genes in hepatocytes and HepG2 cells. Both cell types were treated with PAL (half maximal inhibitory concentration, 22 nmol/L) at a dose of 10, 20, or 40 nmol/L for 24 hours. Messenger RNA analysis showed that the expression levels of *Cyp24a1* and *Sult2a1* were greatly increased by PAL at any dose ($P < .05$ or $P < .01$) (Figure 1F and G). These results suggest that the VDR of hepatocytes can be activated by PAL.

To assess the effect of VDR activation in hepatocytes on cholestatic liver damage, the level of the hepatocyte injury marker alanine aminotransferase (ALT) was measured using a biochemical analysis kit. As shown in Figure 1H, mice at 2 days after BDL had a higher level of serum ALT than sham mice, whereas BDL mice treated with PAL had a significantly decreased ALT level compared with untreated BDL mice ($P < .01$). In addition, PAL also reduced BDL-

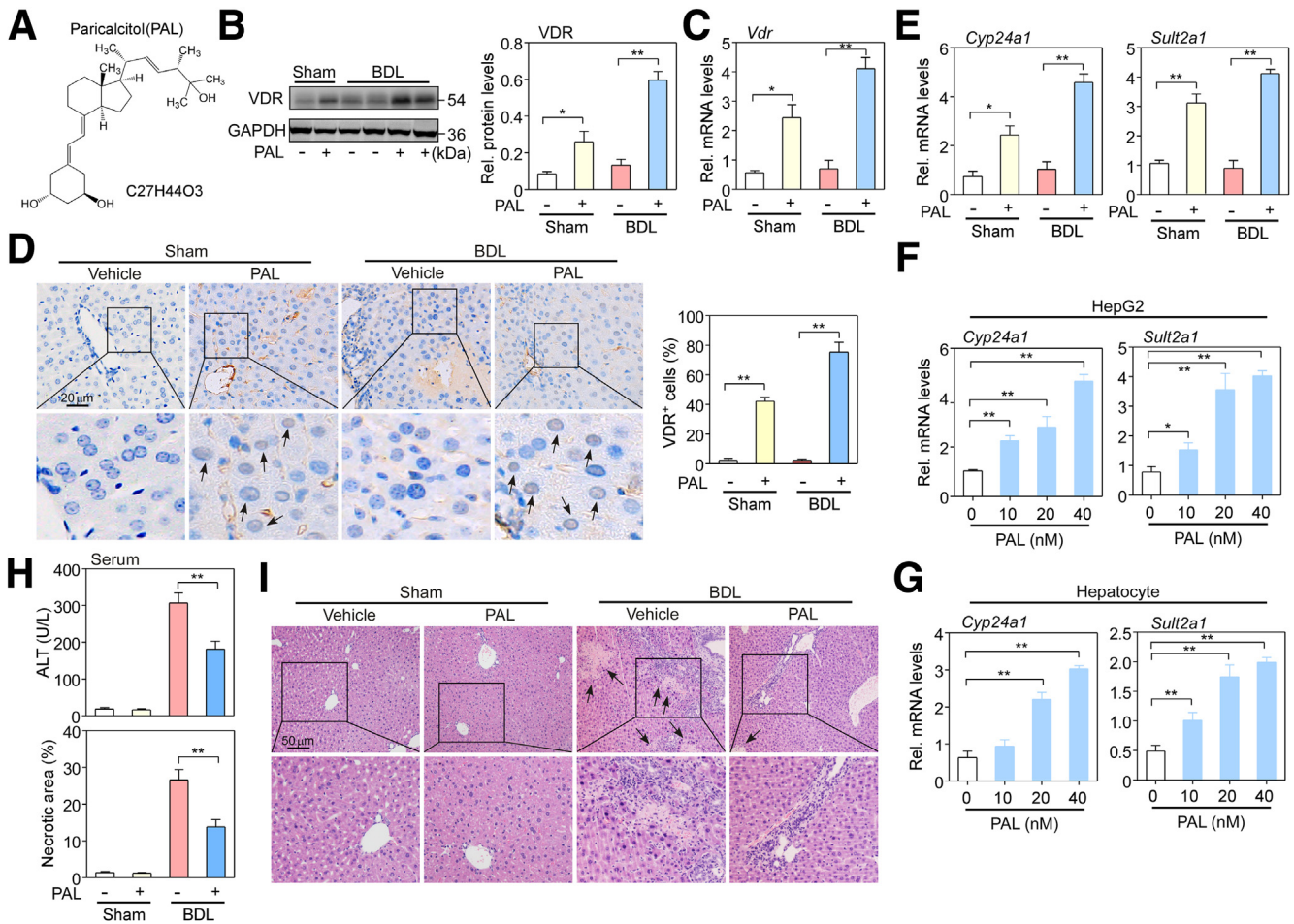


Figure 1. PAL treatment mitigated bile duct ligation–induced hepatic injury in mice. (A) The chemical structure of PAL. (B) Western blot and (C) quantitative PCR assays were used to detect and quantify the protein and messenger RNA (mRNA) expression levels of VDR in isolated primary hepatocytes from sham and BDL mouse liver tissue. $n = 5$. (D) Immunohistochemical staining of VDR was determined in liver sections. *Black arrows* indicate the positive area in the nucleus, and the brown staining area was calculated. $n = 5$. (E) Quantitative PCR assays were used to detect the mRNA levels of the *Vdr* target genes *Cyp24a1* and *Sult2a1* in (F) HepG2 cells and (G) hepatocytes isolated from wild-type C57BL/6 male mice, as described earlier in mice. $n = 3–4$. (H) Liver function was assessed by measuring ALT levels in the serum of mice using commercial kits. $n = 10$. (I) Liver sections from sham and BDL mice at 5 days were subjected to H&E staining, and the liver necrotic area was calculated. *Black arrows* point to necrotic areas in the tissue. $n = 10$. Data are expressed as the means \pm SEM of 3 independent experiments. * $P < .05$, ** $P < .01$ between the indicated groups. GAPDH, glyceraldehyde-3-phosphate dehydrogenase; Rel, relative.

induced liver necrotic area observed by H&E staining ($P < .01$) (Figure 1I). These results suggest that VDR activation in hepatocytes has a protective role during cholestasis.

VDR Activation Suppresses Apoptosis of Hepatocytes by Inhibiting ROS Generation

Bile duct ligation–induced liver injury is associated with cell apoptosis.²⁵ We assessed if VDR activation regulated hepatocyte apoptosis during cholestasis. Apoptosis pathway-related proteins were examined in hepatocytes isolated from sham and BDL mice by Western blot assays. As shown in Figure 2A, BDL led to increases in cleaved-caspase 8, 9, and 3 levels. However, PAL markedly suppressed the increase in cleaved-caspase 9 and 3 levels ($P < .05$ or $P < .01$) but had no effect on cleaved-caspase 8 level, suggesting that the mitochondrial apoptotic pathway may be regulated by PAL. Thus, the

expression of the mitochondrial apoptosis-related proteins Bax, Bcl-2, and cytochrome c was assessed. As expected, Bax and cytochrome c expression levels were greatly increased, while Bcl-2 level was decreased in BDL mice compared with sham mice. However, PAL significantly inhibited the increase in the Bax/Bcl-2 ratio and cytochrome c expression ($P < .05$ or $P < .01$) (Figure 2B). Mitochondrial membrane potential (MMP) depolarization is one of the characteristics of apoptosis. MMP change was examined in hepatocytes isolated from sham and BDL mice by staining with rhodamine 123 (Rho123), a mitochondria-sensitive dye. The results showed that BDL hepatocytes had decreased MMP compared with sham hepatocytes, while PAL reversed this decrease in MMP ($P < .05$) (Figure 2C), suggesting that PAL suppresses apoptosis of hepatocytes via the intrinsic mitochondrial pathway.

BDL triggers ROS accumulation associated with mitochondrial dysfunction,²⁶ and, in turn, ROS can induce cellular

apoptosis.²⁷ We assessed the effect of VDR activation on ROS. ROS levels were observed in sham and BDL mouse livers with a dihydroethidium (DHE) fluorescent probe. The results showed that red fluorescence was seen mainly in hepatic parenchymal cells in BDL mouse liver sections. However, PAL significantly reduced the red fluorescence intensity (Figure 2D). Then, the hepatic oxidative stress marker Ogg1 was analyzed in hepatocytes isolated from sham and BDL mice by Western blot assay. Similar to the fluorescence results, PAL inhibited the BDL-induced increase in Ogg1 expression ($P < .01$) (Figure 2E), suggesting that VDR activation can effectively suppress the BDL-triggered oxidative stress response.

Furthermore, *tert*-butyl hydroperoxide (*t*BHP, 50 μ mol/L) was used to mimic a state of oxidative stress in hepatocytes isolated from C57BL/6 mice and in HepG2 cells. To directly examine if VDR mediates ROS-induced apoptosis of hepatocytes, hepatocytes and HepG2 cells were pretreated with *Vdr* short hairpin RNA (shRNA) or *Vdr* plasmid, followed by *t*BHP. Western blot analysis confirmed that *Vdr* shRNA significantly decreased VDR protein level in hepatocytes and HepG2 cells whereas *Vdr* plasmid markedly increased it (Figure 3A). Then, cell viability was preformed to measure the effects of *Vdr* shRNA and *Vdr* plasmid on cell apoptosis in both hepatocytes and HepG2 cells that already were exposed to *t*BHP. As expected, shRNA-mediated knockdown of *Vdr* enhanced *t*BHP-induced growth inhibition, whereas pretreatment with *Vdr* plasmid abolished this effect on hepatocytes and HepG2 cells ($P < .05$) (Figure 3B). Interestingly, the apoptosis inhibitor ZVADFMK significantly reversed the growth inhibitory effect of *Vdr* shRNA, while the necroptosis inhibitor necrostatin-1 did not remarkably reverse this process ($P < .01$) (Figure 3C). In addition, apoptotic-related proteins were evaluated after addition of the *Vdr* shRNA or *Vdr* plasmid. The results showed that *Vdr* plasmid reduced cleaved-caspase 9 and 3 and Bax levels and increased Bcl-2 level. In contrast, knockdown of VDR reversed these changes in protein expression (Figure 3D).

Because Rac1–NOX1 complex activation can induce ROS generation,²⁸ we assessed the role of VDR activation during ROS generation in hepatocytes isolated from sham and BDL mice by Western blot assay. The results showed that BDL induced an increase in Rac1 and NOX1 levels, whereas PAL markedly suppressed that increase ($P < .05$ or $P < .01$) (Figure 3E). Next, to directly verify whether VDR mediates ROS generation, hepatocytes and HepG2 cells were pretreated with *Vdr* shRNA or *Vdr* plasmid, followed by *t*BHP. Indeed, VDR overexpression greatly reduced Rac1 and NOX1 expression, whereas VDR knockdown abrogated the reduction in their expression in both hepatocytes and HepG2 cells (Figure 3F). In addition, we also observed that the NOX inhibitor apocynin blocked *Vdr* shRNA-induced cell apoptosis in both hepatocytes and HepG2 cells (Figure 3G). These findings suggest that VDR activation suppresses apoptosis through an ROS-dependent Rac1/NOX1 pathway.

VDR Activation Triggers Autophagy of Hepatocytes by Inhibiting ROS

Autophagy appears to be impaired during cholestasis.⁵ In the present study, we assessed whether autophagy was

involved in the reduction in cholestatic liver injury by VDR activation. The generation of autophagosomes was examined in hepatocytes isolated from sham and BDL mice. Western blot analysis showed that BDL significantly increased LC3-I levels but did not affect LC3-II levels compared with sham treatment. In contrast, BDL mice treated with PAL had greatly enhanced conversion of LC3-I to LC3-II compared with BDL mice (Figure 4A). Then, to further confirm the correlation between VDR activation and autophagy during cholestasis, 2 autophagy-related proteins, Beclin-1 and ATG5, which play important roles in autophagy activation and autophagosome assembly, respectively,^{29,30} were detected by Western blot analysis. The results showed that BDL significantly reduced the expression levels of Beclin-1 and ATG5 compared with those in sham mice, while PAL reversed this reduction ($P < .05$ or $P < .01$) (Figure 4A).

To further verify the role of VDR in autophagy during oxidative stress, we assessed autophagosome formation in hepatocytes and HepG2 cells pretreated with *Vdr* shRNA or *Vdr* plasmid with *t*BHP treatment. As expected, the results from Western blot analysis and MAP1LC3A fluorescence staining showed that VDR overexpression markedly enhanced LC3-II conversion, whereas *Vdr* silencing significantly abrogated the conversion of LC3-I to LC3-II in hepatocytes and HepG2 cells ($P < .01$) (Figure 4B and C). Then, the accumulation of autophagosomes and autolysosomes was analyzed by acridine orange (AO) staining. AO has a weak base that freely passes across the plasma membrane in a neutral state distinguished by green fluorescence. After entrance into acidic compartments, AO changes into the protonated form, which is distinguished by bright red fluorescence. As shown in Figure 4D, the intensity of the bright red fluorescence was lower in *Vdr*-silenced cells but was higher in *Vdr* plasmid cells. Moreover, autophagy-related proteins also were examined. Western blot analysis showed that VDR knockdown inhibited the expression of ATG5 and Beclin-1 in both cell lines. In contrast, the expression of these 2 proteins was increased significantly in VDR-overexpressing cells (Figure 4E).

Next, we assessed autophagic flux in hepatocytes isolated from sham and BDL mice. The autophagy-specific substrate sequestosome 1 (SQSTM1)/p62 is a major indicator of autophagic flux. SQSTM1 accumulates when autophagy is inhibited and is decreased when there is autophagic flux.³¹ The Western blot analysis results showed that BDL increased the SQSTM1 protein level, whereas PAL decreased it ($P < .01$) (Figure 4F). This result was verified in *Vdr* shRNA- and *Vdr* plasmid-treated cells after *t*BHP treatment. As expected, VDR knockdown increased SQSTM1 protein levels, while the *Vdr* plasmid decreased its expression in both cell lines (Figure 4G). Moreover, we observed an increase in LC3-II levels in HepG2 cells transfected with the *Vdr* plasmid followed by chloroquine treatment compared with cells transfected with the *Vdr* plasmid alone, suggesting that autophagic flux was increased in VDR-overexpressing HepG2 cells ($P < .01$) (Figure 4H). Collectively, these findings suggest that VDR activation has an important role in autophagy-lysosome pathways.

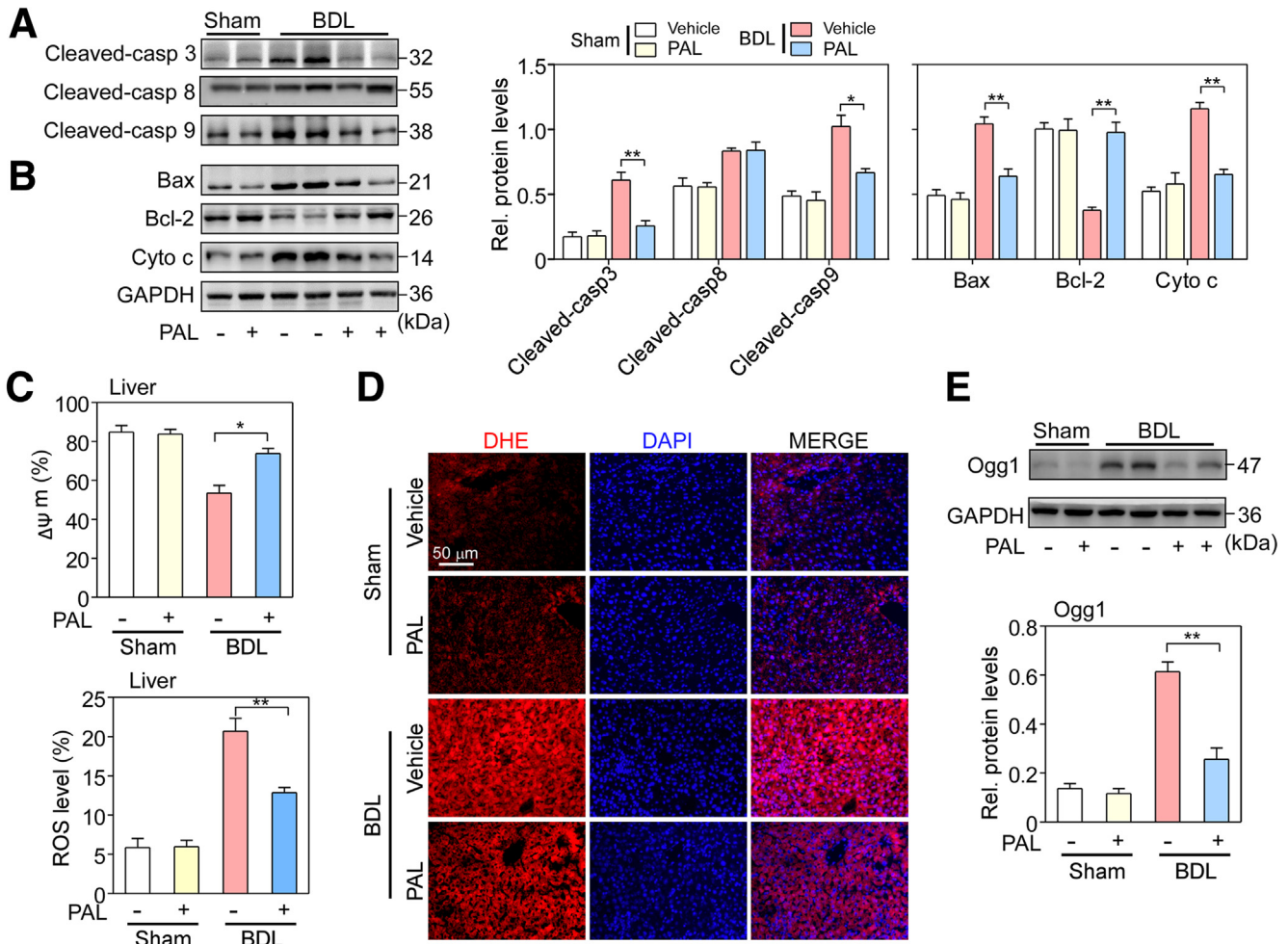


Figure 2. VDR activation suppressed bile duct ligation-induced apoptosis of hepatocytes. (A) Expression levels of apoptosis proteins, including cleaved-caspase 8, 9, and 3, and (B) the mitochondrial apoptosis-related proteins Bax, Bcl-2, and cytochrome c in hepatocytes isolated from sham and BDL mice were determined by Western blot analysis and quantified. $n = 5$. (C) MMP depolarization was examined by Rho123 staining in hepatocytes isolated from sham and BDL mice. $n = 5$. (D) ROS levels were observed in sham and BDL mouse livers by a DHE fluorescent probe. Cell nuclei were stained with 4',6-diamidino-2-phenylindole (DAPI). $n = 5$. (E) Hepatic oxidative stress marker Ogg1 protein expression in hepatocytes isolated from sham and BDL mouse livers was determined by Western blot analysis and quantified. $n = 5$. Data are expressed as the means \pm SEM of 3 independent experiments. * $P < .05$, ** $P < .01$ between the indicated groups. GAPDH, glyceraldehyde-3-phosphate dehydrogenase; Rel, relative.

Inhibition of Apoptosis by VDR Activation Is Associated With Autophagy Activation

A study has shown that autophagy activation inhibits cell apoptosis.³² To investigate whether autophagy activation mediates VDR activation-inhibited apoptosis, we used *Atg5* small interfering RNA (siRNA) to block autophagosome formation and an *Atg5* plasmid to induce autophagy. Western blot analysis verified that *Atg5* siRNA significantly decreased LC3-II levels, while the *Atg5* plasmid increased LC3-II conversion (Figure 5A). Next, we measured cell viability when *Atg5* was knocked down by specific siRNA. Indeed, after entering the logarithmic growth period of cells on day 4, siRNA-mediated knockdown of *Atg5* gradually showed the effect of promoted *tBHP*-induced growth inhibition, especially on day 10, compared with control siRNA. In contrast, up-regulation of LC3-II expression by the *Atg5* plasmid prevented *tBHP*-induced growth inhibition

compared with control vector on day 10 in both hepatocytes and HepG2 cells ($P < .05$) (Figure 5B). Interestingly, the *Vdr* plasmid showed synergistic blocking effects on *tBHP*-induced growth inhibition in the presence of the *Atg5* plasmid. However, VDR overexpression did not dramatically block growth inhibition by *tBHP* in the presence of *Atg5* knockdown (Figure 5B), suggesting that VDR activation contributes to apoptosis via an autophagy-dependent mechanism.

Then, several apoptosis-related proteins, cleaved-caspase 9 and 3, Bax and Bcl-2, were examined in hepatocytes and HepG2 cells co-treated with *Atg5* siRNA and the *Vdr* plasmid. Similarly, pretreatment with *Atg5* siRNA significantly enhanced the *tBHP*-induced increase in cleaved caspase 9 and 3 and Bax and the decrease in Bcl-2 in the absence or presence of the *Vdr* plasmid. In contrast, cells co-treated with the *Atg5* plasmid and *Vdr* plasmid showed the

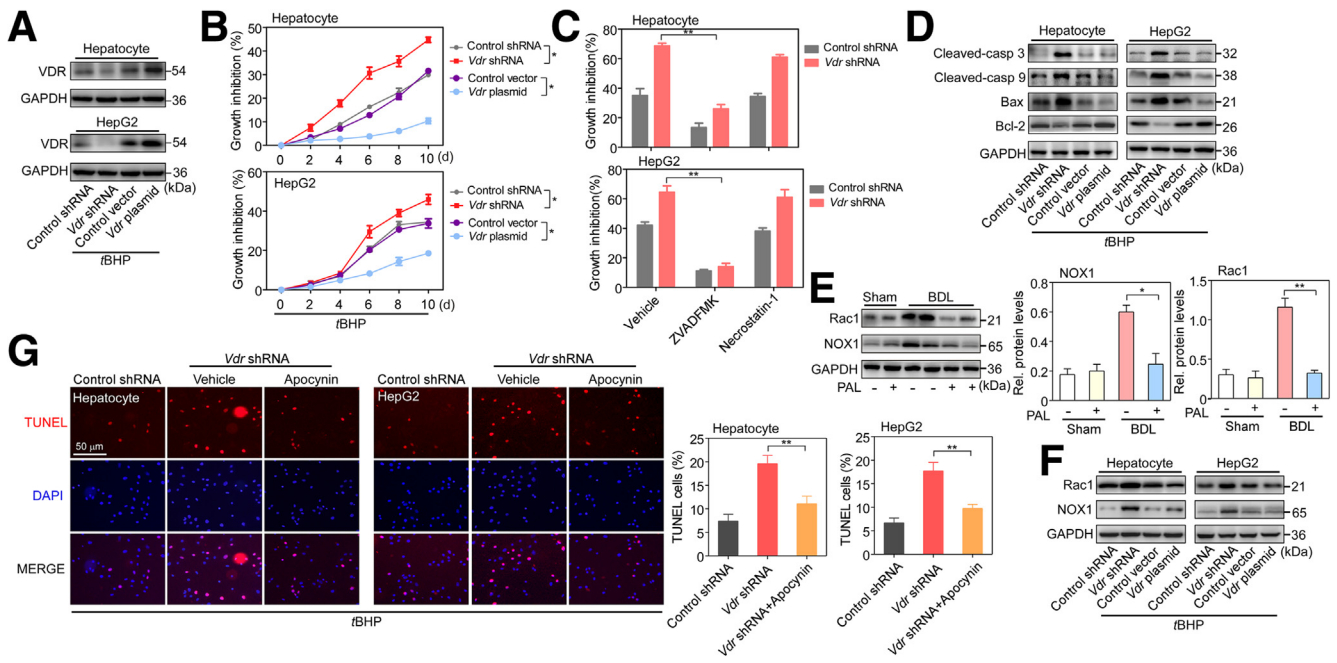


Figure 3. VDR regulated apoptosis of hepatocytes dependent on the inhibition of the RAC1/NOX1 pathway. (A) Hepatocytes isolated from wild-type C57BL/6 mice and HepG2 cells were transfected with *Vdr* shRNA or *Vdr* plasmid, followed by *t*BHP treatment (50 μ mol/L) for 24 hours. The transfection efficiency was confirmed by Western blot analysis. $n = 3$. (B) Cell viability was assayed using CCK8 kits. $n = 3$. (C) Hepatocytes and HepG2 cells in the presence of *Vdr* shRNA were treated with ZVAD-FMK (10 μ mol/L) and necrostatin-1 (10 μ mol/L), and cell viability was assayed. $n = 3$. (D) The levels of the apoptotic-related proteins cleaved-caspase 3 and 9, Bax, and Bcl-2 were examined by Western blot analysis. $n = 3-4$. (E) Rac1 and NOX1 protein expression levels in hepatocytes isolated from sham and BDL mouse livers were determined by Western blot analysis and quantified. $n = 5$. (F) Rac1 and NOX1 protein expression levels were examined in hepatocytes and HepG2 cells with *Vdr* shRNA or *Vdr* plasmid after *t*BHP treatment. $n = 3$. (G) Hepatocytes and HepG2 cells in the presence of *Vdr* shRNA were treated with the NOX inhibitor apocynin (10 μ mol/L), and then TUNEL staining was performed. Cell nuclei were stained with 4',6-diamidino-2-phenylindole (DAPI). $n = 5$. Data are expressed as the means \pm SEM of 3 independent experiments. * $P < .05$, ** $P < .01$ between the indicated groups. GAPDH, glyceraldehyde-3-phosphate dehydrogenase; Rel, relative.

opposite effect on apoptosis-related protein expression (Figure 5C).

In addition, terminal deoxynucleotidyl transferase-mediated deoxyuridine triphosphate nick-end labeling (TUNEL) staining was performed in hepatocytes and HepG2 cells. When cells were cotreated with *Atg5* siRNA and the *Vdr* plasmid, *Atg5* knockdown increased the number of TUNEL-positive cells, but the *Vdr* plasmid did not significantly eliminate the increase in TUNEL-positive cells in the presence of *Atg5* knockdown. In contrast, pretreatment with the *Atg5* plasmid remarkably inhibited the number of TUNEL-positive cells after *t*BHP treatment, and the *Vdr* plasmid showed a synergistic effect with the *Atg5* plasmid (Figure 5D). Overall, these results indicate that activation of autophagy is required for VDR activation to suppress apoptosis in vitro.

VDR Activation Inhibits Apoptosis and Activates Autophagy via the ROS-Dependent ERK and p38MAPK Pathways

ROS generation through the Rac1/NOX1 pathway can activate ERK and p38MAPK, leading to the induction of apoptosis.^{28,33} Rac1 and ERK expression were correlated

negatively with autophagic flux.^{34,35} We assessed the role of VDR activation in the ROS-dependent activation of stress kinases in BDL mice. As expected, BDL activated phosphorylation of ERK1/2 and p38MAPK, whereas PAL exerted an inhibitory effect on phosphorylation of ERK1/2 and p38MAPK (Figure 6A). Moreover, this result was confirmed in hepatocytes and HepG2 cells treated with *Vdr* siRNA and *Vdr* plasmid. Western blot analysis showed that both ERK1/2 and p38MAPK were activated by phosphorylation upon *t*BHP treatment. *Vdr* siRNA enhanced their phosphorylation, but the *Vdr* plasmid reversed that effect (Figure 6B). Pretreatment of cells with an inhibitor of p38MAPK (SB202190) significantly increased the LC3-II level and decreased the number of apoptotic cells induced by *t*BHP in the presence of *Vdr* siRNA. However, the MAPK and Mitogen-activated protein kinase kinase (MEK)/ERK activator C16-Platelet activating factor reversed these results in the presence of *Vdr* overexpression ($P < .01$) (Figures 6C and 7A). In addition, the ROS scavenger NAC was used to examine whether the inhibitory effect of VDR activation on the activation of ERK and p38MAPK may be ROS-dependent. The results showed that NAC blocked ERK activation and inhibited the activation of p38MAPK in the presence of *Vdr* knockdown (Figure 7B). Together, these results show that

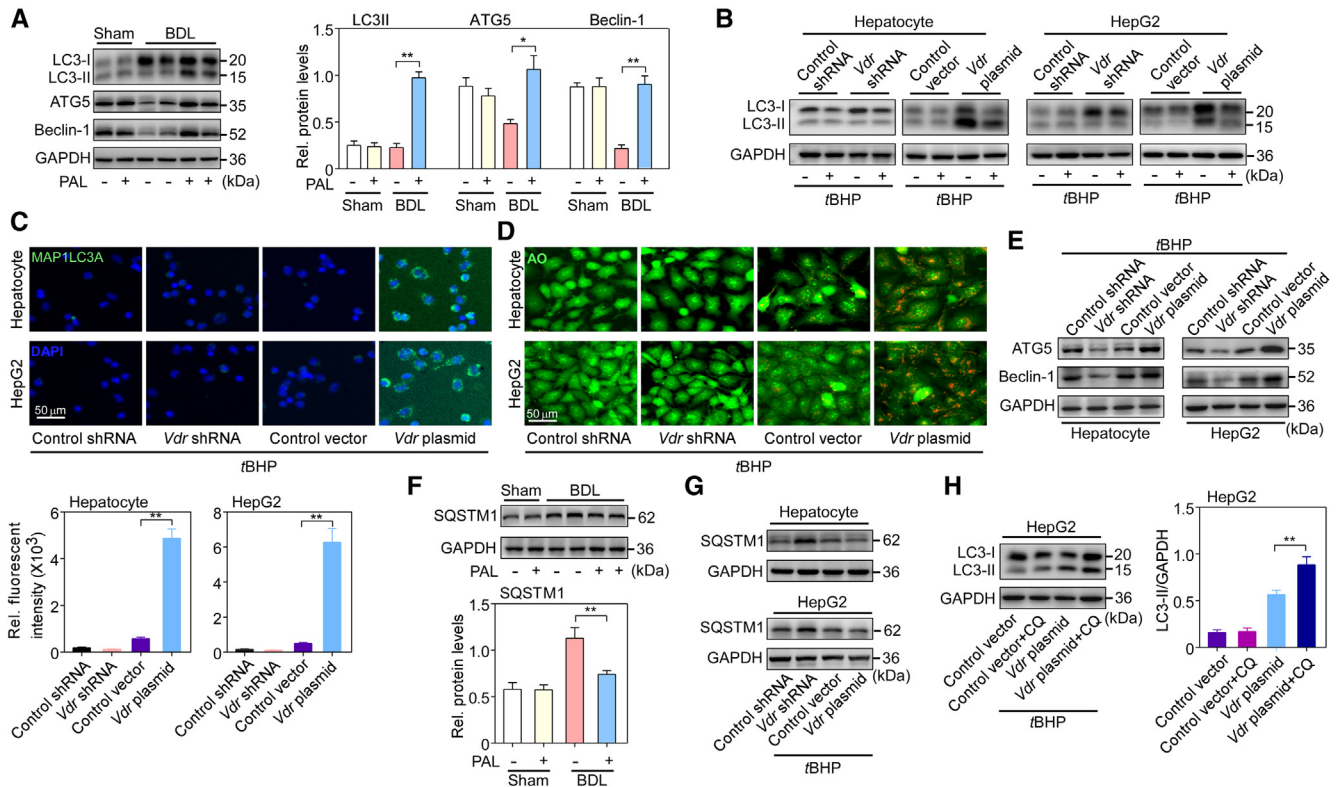


Figure 4. VDR activation triggers autophagy in hepatocytes by inhibiting ROS. (A) Autophagy-related proteins LC3-I and II, ATG5, and Beclin-1 in hepatocytes isolated from sham and BDL mouse livers were identified by Western blot analysis and quantified. $n = 5$. (B) LC3-I and LC3-II protein expression levels were determined by Western blot analysis in hepatocytes isolated from wild-type C57BL/6 mice and HepG2 cells in the presence of *Vdr* shRNA or *Vdr* plasmid treated with or without *tBHP*. $n = 3-4$. (C) Representative images of MAP1LC3A-stained hepatocytes and HepG2 cells in the presence of *Vdr* shRNA or *Vdr* plasmid treated with *tBHP*. Cell nuclei were stained with 4',6-diamidino-2-phenylindole. $n = 3$. (D) Autophagosomes and autolysosomes stained with AO in hepatocytes and HepG2 cells in the presence of *Vdr* shRNA or *Vdr* plasmid treated with *tBHP*. Green color intensity shows the cytoplasm and nucleus, while red color intensity shows autophagosomes and autolysosomes. (E) The levels of the autophagy-related proteins ATG5 and Beclin-1 in hepatocytes and HepG2 cells in the presence of *Vdr* shRNA or *Vdr* plasmid treated with *tBHP* were determined by Western blot analysis. $n = 3$. (F) Protein expression of the autophagy-specific substrate SQSTM1/p62 was determined by Western blot analysis in hepatocytes isolated from sham and BDL mouse livers and quantified. $n = 5$. (G) SQSTM1/p62 protein expression was determined by Western blot analysis in hepatocytes and HepG2 cells in the presence of *Vdr* shRNA or *Vdr* plasmid treated with *tBHP*. (H) LC3-I and LC3-II expression in HepG2 cells in the presence of *Vdr* plasmid pretreated with chloroquine (CQ) (10 $\mu\text{mol/L}$) for 30 minutes followed by *tBHP* treatment. $n = 5$. Data are expressed as the means \pm SEM of 3 independent experiments. $*P < .05$, $**P < .01$ between the indicated groups. GAPDH, glyceraldehyde-3-phosphate dehydrogenase; Rel, relative.

VDR activation contributes to the inhibition of the ROS-dependent ERK and p38MAPK pathways.

Discussion

Autophagy and apoptosis are involved in the pathogenesis of cholestasis. Bile duct ligation directly triggers hepatocyte apoptosis but impairs autophagy. However, activation of autophagy can alleviate liver injury in BDL mice,⁵ which provides a new therapeutic opportunity for cholestasis. In this article, we provide evidence supporting the protective role of VDR activation-mediated autophagy and apoptosis during cholestasis, as follows: (1) treatment with PAL up-regulated VDR expression in mouse liver hepatocytes and human HepG2 cells; (2) up-regulation of VDR inhibited BDL/*tBHP*-triggered hepatocyte apoptosis in an autophagy-dependent manner by suppressing ROS generation; and (3)

BDL/*tBHP*-impaired autophagic flux can be reversed by up-regulation of VDR via inhibition of ROS-dependent activation of the ERK/p38MAPK pathway.

Vitamin D deficiency is associated with an increased incidence of chronic cholestatic diseases, such as primary biliary cirrhosis and primary sclerosing cholangitis,^{36,37} thereby suggesting its hepatoprotective role. The biological effects of vitamin D are mediated mainly by VDR, a member of the nuclear hormone receptor superfamily.³⁸ VDR activation in hepatic stellate cells delays hepatic fibrosis by inhibiting the transforming growth factor- β /Smad signaling pathway in CCl₄ mice,³⁹ whereas the lack of VDR through genetic knockout in cholangiocytes aggravates liver injury by disrupting the tight junctions of biliary epithelial cells in BDL mice.⁸ Moreover, activation of VDR in macrophages by vitamin D ligand ameliorates liver steatosis and insulin resistance in nonalcoholic fatty liver disease.²³ However, the

role of VDR in hepatocytes in cholestasis remains unclear. Although VDR expression is very low in hepatocytes, treatment with PAL up-regulated the expression of VDR and its downstream target genes *Cyp24a1* and *Sult2a1* both in hepatocytes of mouse liver and human HepG2 cells. Meanwhile, PAL improved BDL-induced hepatocyte damage, suggesting that VDR activation of hepatocytes exerts a hepatoprotective role during cholestasis.

In chronic liver disease, hepatic apoptosis is considered to be a prominent pathologic feature in most forms of liver injury. Interventions in hepatic apoptosis can delay disease progression and reduce the morbidity of liver disease. However, hepatic apoptosis can be regulated by autophagic activity. Autophagy removes damaged mitochondria in a process termed *mitophagy*. Mitophagy can reduce mitochondria-derived ROS formation and the release of pro-cell death factors from mitochondria. Consistent with this observation, ROS production from mitochondria can be suppressed by rapamycin treatment but exacerbated by chloroquine treatment.⁴⁰ Autophagy influences mitochondrial recycling and thus can modulate hepatic apoptosis via the mitochondrial pathway. Furthermore, autophagy is identified as an upstream mechanism in apoptosis inhibition by preventing mitochondrial outer-membrane permeabilization and the subsequent release of proapoptotic molecules, such as cytochrome *c*.⁴¹ In contrast, apoptosis effector molecules can suppress autophagy.⁴² Indeed, crosstalk exists between autophagy and apoptosis and is manifested by regulatory genes that act in common pathways. These regulatory genes include p53, Atg5, and Bcl-2. The autophagic protein Atg5 can interact with Fas-associated protein with death domain to stimulate extrinsic apoptosis pathways and induce apoptotic death, and this can be blocked by the pan caspase inhibitor ZVADFMK.⁴³ Therefore, the cytoprotective function of autophagy involves negative modulation of apoptosis and vice versa.

A complex interplay between hepatic autophagy and apoptosis determines the degree of hepatic apoptosis and the progression of liver disease, as shown by preclinical models and clinical trials.⁴⁴ During cholestasis, the pathologic features of the liver showed increased cell apoptosis and impaired autophagy. Thus, regulation of the crosstalk between autophagy and apoptosis may be an effective approach for the treatment of cholestatic liver disease. Several reports have shown that VDR activation by vitamin D ligand can reduce cell apoptosis in various types of cells, including renal tubular epithelial cells and intestinal epithelial cells,^{45,46} and can regulate autophagy to attenuate foam cell formation in macrophages.⁴⁷ In contrast, the lack of VDR led to an imbalance of autophagy and apoptosis in the intestinal epithelium.⁴⁸ Interestingly, in this study, we found that up-regulation of VDR expression in hepatocytes inhibited bile duct ligation-induced hepatocyte apoptosis characterized by decreased cleaved caspase 9 and 3 levels, but did not affect cleaved caspase 8 level. According to this result, we further found that up-regulation of VDR inhibited hepatocyte apoptosis via the intrinsic mitochondrial pathway. Similarly, upon hepatocyte exposure to the OS-inducing compound *tBHP*, *Vdr* silencing enhanced

hepatocyte apoptosis, whereas *Vdr* overexpression led to apoptosis resistance. Meanwhile, up-regulated VDR expression also appeared to increase autophagosome formation and autophagic flux, which was the underlying VDR-dependent mechanism of apoptosis inhibition in both BDL mice and human HepG2 cells. Disruption of autophagy by *Atg5* siRNA impaired VDR plasmid-inhibited apoptosis. This result indicates a novel function of VDR in addition to controlling inflammation, apoptosis, and proliferation in hepatic diseases. Although our data suggest a direct connection between autophagy and up-regulated VDR-inhibited hepatocyte apoptosis, we could not eliminate other effects that may mediate this inhibiting effect.

Recently, it was reported that ROS are key regulatory molecules in crosstalk between apoptosis and autophagy.⁴⁹ Controlling ROS levels significantly reduces apoptosis by inducing autophagy in human umbilical vein endothelial cells, thereby preventing atherosclerosis.⁵⁰ Meanwhile, inhibition of ROS promotes mitophagy and reduces apoptosis associated with mitochondria-dependent pathways, thereby attenuating spinal cord ischemia-reperfusion injury in mice.⁵¹ BDL causes the body to produce a large amount of ROS, leading to cholestatic liver injury.⁵² VDR was shown to have antioxidant properties, and VDR activation through inhibition of ROS generation was shown to prevent high-glucose-induced endothelial cell apoptosis, ameliorating diabetes-related endothelial dysfunction in diabetic mice.⁵³ Consistent with this observation, our results show that VDR activation in hepatocytes by PAL or *Vdr* plasmid inhibited ROS generation under a stress condition. Although VDR activation inhibited ROS generation in our studies, the mechanisms of BDL triggering of ROS generation are complicated. In addition, our study showed that ROS production depends on the activation of the Rac1-NOX1 complex.¹⁴ Rac1/NOX1 is activated under stress conditions, causing ROS generation and consequential neuronal death in dopaminergic neurons in the substantia nigra of mice.⁵⁴ Inhibiting the expression of Rac1 and NOX1 can inhibit ROS generation to alleviate bile duct ligation-induced liver injury in rats.¹⁵ Here, we show that up-regulation of VDR inhibited the activation of Rac1/NOX1 induced by ROS in primary hepatocytes and HepG2 cells, and this was confirmed by comparison with the effect of apocynin (a NOX inhibitor). Moreover, apocynin also blocked *Vdr* knockdown-induced apoptosis, suggesting that VDR activation inhibits ROS-induced apoptosis by suppressing the activation of the Rac1/NOX1 pathway.

In addition, ROS can stimulate the activation of the ERK and p38MAPK signaling pathways.⁵⁵ Inhibition of ROS-activated p38MAPK and ERK pathways reduces renal tubular epithelial cell apoptosis and alleviates renal fibrosis induced by unilateral ureteral obstruction,⁵⁶ and inhibiting ROS-mediated ERK signaling can reduce Madin-Darby canine kidney cells apoptosis to further alleviate ischemia-reperfusion-induced acute kidney injury.⁵⁷ Moreover, activation of ROS-mediated ERK/p38 MAPK-dependent signaling inhibits autophagy and promotes cell apoptosis in human prostate cancer cells, thereby alleviating prostate cancer progression.¹⁷ In liver, the ERK/p38MAPK signaling

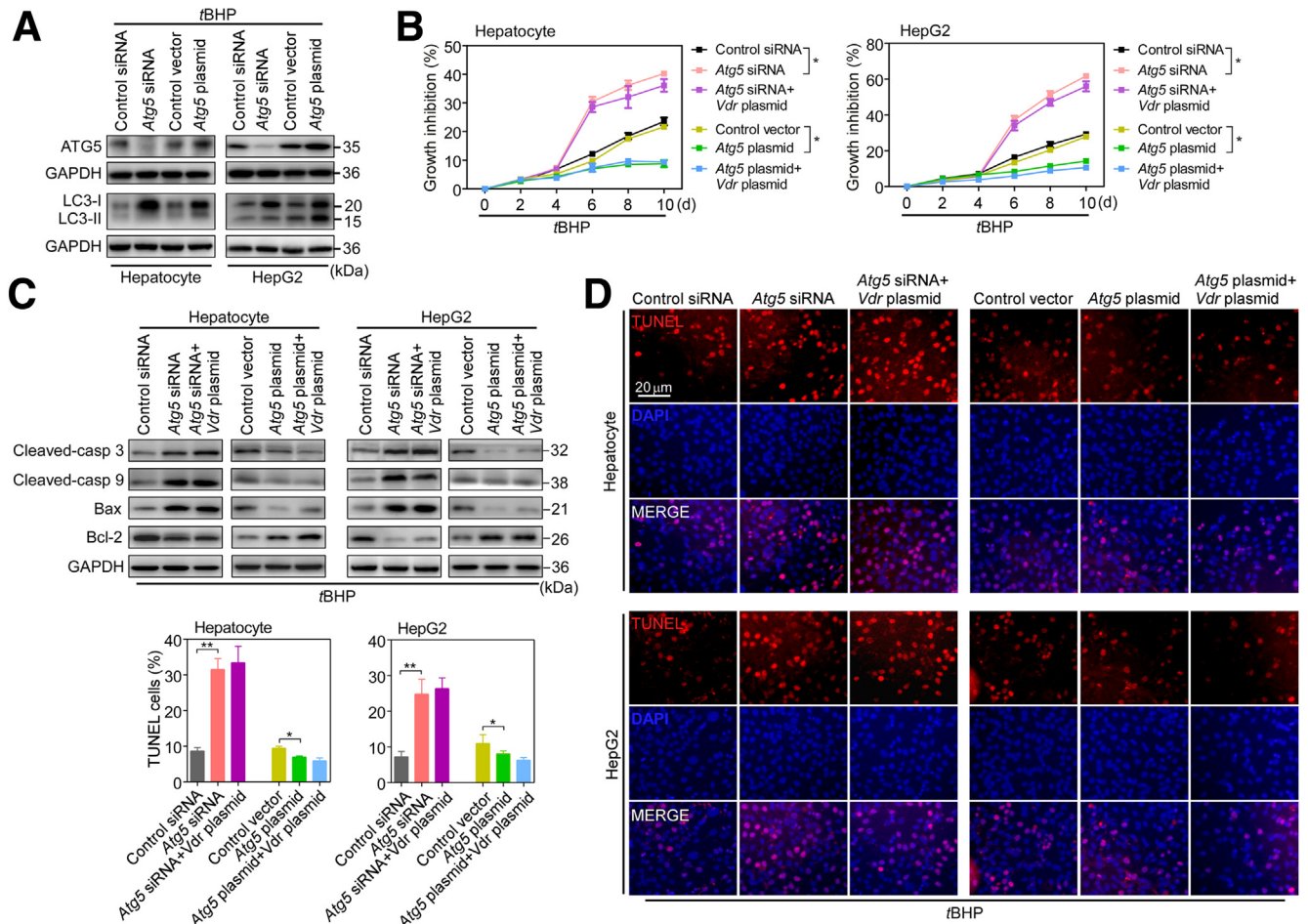


Figure 5. Inhibition of apoptosis by VDR activation is associated with autophagy activation. (A) ATG5 and LC3-I and LC3-II protein expression levels were determined by Western blot analysis in hepatocytes and HepG2 cells in the presence of Atg5 siRNA or Atg5 plasmid treated with tBHP. $n = 3$. (B) Cell viability. (C) The levels of the apoptosis-related proteins cleaved-caspase 3 and 9, Bax, and Bcl-2 were determined and (D) TUNEL staining was performed in hepatocytes and HepG2 cells in the presence of Atg5 siRNA/Atg5 plasmid or Atg5 siRNA/Atg5 plasmid + *Vdr* plasmid followed by tBHP treatment. $n = 3-4$. Cell nuclei were stained with 4',6-diamidino-2-phenylindole (DAPI). Data are expressed as the means \pm SEM of 3 independent experiments. * $P < .05$ and ** $P < .01$ between the indicated groups. GAPDH, glyceraldehyde-3-phosphate dehydrogenase.

pathway was significantly activated in a bile duct ligation-induced acute cholestasis model,⁵⁸ which in turn caused ROS accumulation and cell apoptosis in the gut and liver, thereby aggravating cholestatic liver injury in rats.¹⁸ Interestingly, we found that up-regulation of VDR expression inhibited the activation of ERK and p38MAPK by blocking their phosphorylation. This is consistent with previous research that vitamin D/VDR signaling blocks the activation of p38MAPK and ERK and inhibits podocyte apoptosis to protect the kidney from diabetic damage in mice.²⁰ In addition, a study showed that activation of p38MAPK inhibits the expression of LC3-II and ATG5, leading to reduction of autophagosome formation and autophagic flux and induction of apoptosis in chicken embryonic fibroblasts.⁵⁹ In addition, activation of ERK impairs autophagic flux and promotes apoptosis in human colorectal cancer HT-29 and HCT116 cells.⁶⁰ Consistent with our study, inhibition of p38MAPK activation induces a decrease in the level of cleaved-caspase 3 and an increase in the level

of LC3-II, which reversed the effect of *Vdr* knockdown, whereas activation of ERK reversed the effect of *Vdr* over-expression on apoptosis and autophagy in primary hepatocytes and HepG2 cells. Our data suggest that regulation of hepatocyte apoptosis and autophagy by VDR activation occurs via the p38MAPK/ERK pathway. Moreover, NAC blocked the activation of p38MAPK and ERK induced by *Vdr* knockdown. This finding indicates that regulation of the ERK/p38MAPK pathway by VDR activation is ROS-dependent during cholestasis.

In conclusion, we show that bile duct ligation-triggered hepatocyte apoptosis is inhibited by up-regulating VDR expression through suppressing ROS generation by inhibiting the RAC1-NOX1 complex. Up-regulating VDR-inhibited apoptosis is autophagy-dependent and occurs through inhibition of the activation of the ROS-dependent ERK/p38MAPK pathway, resulting in mitigation of cholestatic liver injury (Figure 8). Therefore, our results point to new therapeutic approaches for cholestatic liver injury.

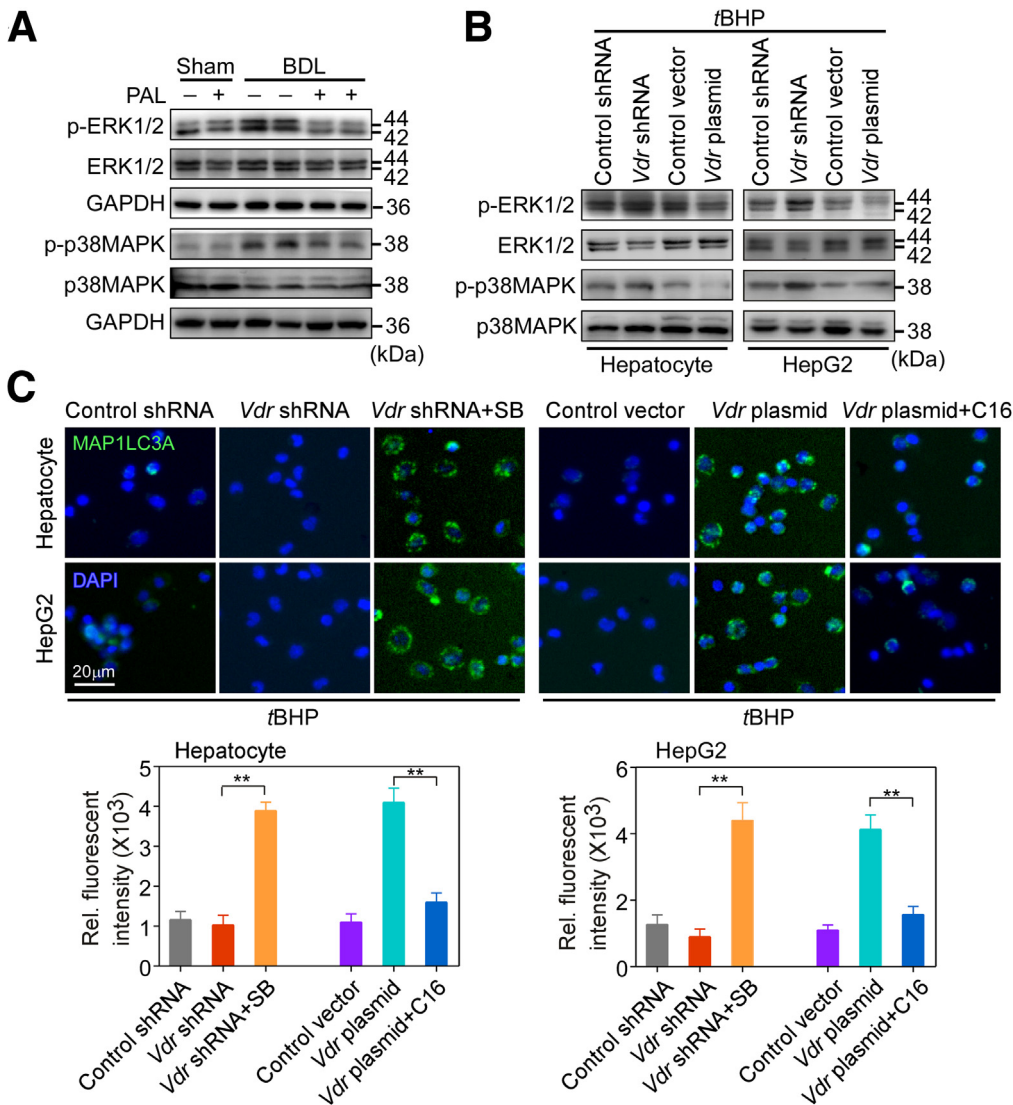


Figure 6. VDR mediated ROS-induced autophagy via the ERK and p38MAPK pathways. (A) ERK1/2 and p38MAPK and their phosphorylation were examined by Western blot analysis in hepatocytes isolated from sham and BDL mouse livers. $n = 5$. (B) ERK1/2 and p38MAPK and their phosphorylation were examined by Western blot analysis in hepatocytes and HepG2 cells in the presence of *Vdr* shRNA or *Vdr* plasmid treated with *tBHP*. $n = 3$. (C) Representative images of MAP1LC3A-stained and hepatocytes and HepG2 cells in the presence of *Vdr* shRNA or *Vdr* plasmid treated with an inhibitor of p38MAPK (SB202190, 10 $\mu\text{mol/L}$) or the MAPK and MEK/ERK activator (C16-PAF, 1 $\mu\text{mol/L}$) after *tBHP* treatment. Cell nuclei were stained with 4',6-diamidino-2-phenylindole (DAPI). $n = 3$. Data are expressed as the means \pm SEM of 3 independent experiments. ** $P < .01$ between the indicated groups. GAPDH, glyceraldehyde-3-phosphate dehydrogenase; Rel, relative; SB, SB202190.

Materials and Methods

Animal Experimental Models

This study was conducted after approval by the Animal Research Committee of Taizhou University and followed the Animal Research: Reporting of In Vivo Experiments (ARRIVE) guidelines pertaining to animal experimentation. Eight- to 10-week-old weight-matched healthy C57BL/6 male mice were purchased from Nanjing Junke Biotechnology Corporation, Ltd (Nanjing, Jiangsu, China). The mice were placed in specific pathogen-free conditions ($22^{\circ}\text{C} \pm 1^{\circ}\text{C}$) under a 12-hour light-dark cycle with free access to food and water. Mice were fasted for 12 hours before the common BDL and drank water freely. The common BDL was as previously described.⁹ Briefly, mice were anesthetized with 2% isoflurane (Ruiwode Life Technology Co, Ltd, Shenzhen, China) and were fixed on an animal operating table with a heating pad (37°C). After a midline laparotomy, the common bile duct was separated from the surrounding tissues, and dissociated between the 2 ligatures with 6-0 nylon suture. The sham group mice underwent the

same procedure, including separating the bile duct but without ligation. Mice were randomly pretreated intraperitoneally with PAL (200 ng/kg, every other day; Sigma-Aldrich, St Louis, MO) or vehicle (propylene glycol) for 3 days before BDL and then with PAL for 5 days after surgery. Five days later, animals were given an overdose of pentobarbital sodium by intraperitoneal injection. Liver tissues and serum were collected from the BDL and sham mice and stored at -80°C .

Histologic Analysis and Immunostaining

The livers from sham and BDL mice were removed, and fixed in 4% paraformaldehyde (PFA) (#158127; Sigma-Aldrich) for 24 hours at 20°C . Then, samples were dehydrated using increasing concentrations of ethanol and embedded in paraffin. The sections were deparaffinized and stained using H&E to observe the pathologic manifestations of the liver tissues of each group of mice.

For immunohistochemistry staining, paraffin sections (4 micrometer) of liver tissue were incubated in citrate buffer

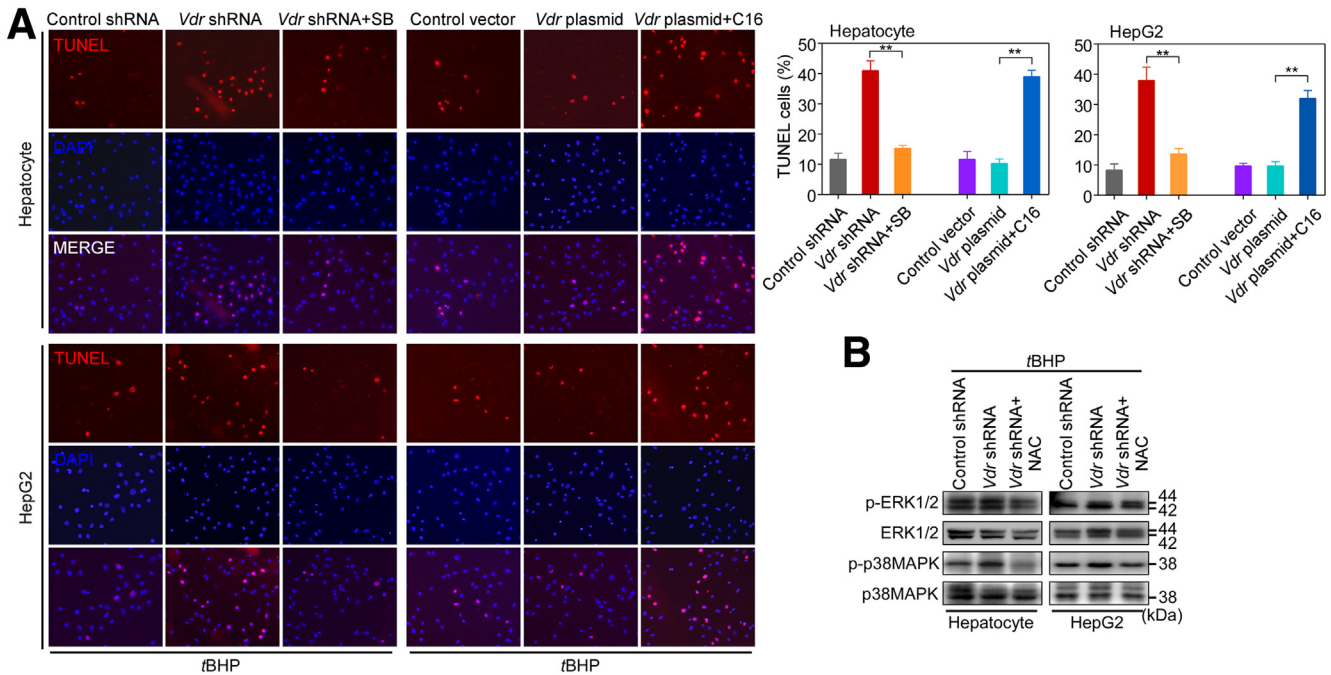


Figure 7. VDR inhibits apoptosis through the ROS-dependent ERK and p38MAPK pathways. (A) Representative images of TUNEL-stained hepatocytes and HepG2 cells in the presence of *Vdr* shRNA or *Vdr* plasmid treated with an inhibitor of p38MAPK (SB202190, 10 μ mol/L) or the MAPK and MEK/ERK activator (C16-PAF, 1 μ mol/L) after tBHP treatment. Cell nuclei were stained with 4',6-diamidino-2-phenylindole (DAPI). $n = 3$. (B) ERK1/2 and p38MAPK and their phosphorylation were examined by Western blot analysis in hepatocytes and HepG2 cells in the presence of *Vdr* shRNA or *Vdr* shRNA+ NAC (5 mmol/L) after tBHP treatment. $n = 3$. Data are expressed as the means \pm SEM of 3 independent experiments. ** $P < .01$ between the indicated groups.

(pH 6.0) for 5 minutes at 108°C for antigen retrieval and then subjected to 3% H₂O₂ in phosphate-buffered saline (PBS) for 15 minutes at room temperature to quench endogenous peroxidase activity. After blocking with 5% bovine serum albumin (BSA) to prevent nonspecific antigen binding, sections were incubated with antibody for VDR (1:100, #ab109234; Abcam, Cambridge, UK) at 4°C overnight and then incubated with biotinylated secondary anti-rabbit antibody (#PV-6001; ZSGB Biotech Co, Beijing, China) in the dark at room temperature for 1 hour, followed by visualization with 3,3'-diaminobenzidine tetrachloride and counterstaining with hematoxylin.

For immunofluorescence staining, cells on glass coverslips were fixed by 4% PFA for 15 minutes. Then 5% BSA was used to block nonspecific antigen binding for 1 hour. Cells were incubated with antibody for MAP1LC3A (1:100, #ab52768; Abcam) at 4°C overnight and then incubated with secondary anti-rabbit antibody (#A32731, 1:200; Invitrogen, Carlsbad, CA) in the dark at room temperature for 30 minutes. Mounted on slides with mounting medium with 4',6-diamidino-2-phenylindole (#H-1200; Vector Labs, Burlingame, CA). All images were acquired using a digital image-capture system (CX40; Olympus, Tokyo, Japan) to collect photographs.

DHE Staining

The mouse liver was fixed in 4% PFA and dehydrated with 30% sucrose, and then cut into 5- μ m slices. The sections

were incubated in DHE dye (1 μ mol/L, #S0063; Beyotime Institute of Biotechnology, Beijing, China) for 1 hour in the dark at room temperature. Then, the sections were washed 4 times with PBS (pH 7.2) and mounted on slides with mounting medium with 4',6-diamidino-2-phenylindole (#H-1200; Vector Labs). Then, an Olympus fluorescence microscope (DP730) was used to observe and take images.

Cell Culture and Drug Treatment

HepG2 cells were purchased from the Shanghai Institute of Biological Science (Shanghai, China). The cells were cultured in Dulbecco's modified Eagle medium (DMEM) (#12491-015; Gibco, Carlsbad, CA) containing 10% heat-inactivated fetal bovine serum (#10099141; Gibco) and 1% penicillin/streptomycin (#15640055; Gibco). The cells were maintained at 37°C under a humidified atmosphere of 5% CO₂ and 95% air and were grown as a contact-inhibited monolayer. The cells from each flask were detached with 0.05% trypsin, resuspended in fresh medium, and cultured on glass coverslips for immunostaining or 100-mm dishes for Western blot analysis.

The primary hepatocyte was isolated from the liver of a 6-week-old male C57BL/6 mouse according to a reported protocol.²⁰ Briefly, mice were anesthetized and after intubation in the portal vein, the livers were perfused in situ with Ca²⁺- and Mg²⁺-free Hank's balanced saline solution supplemented with 0.5 mmol/L ethylene glycol-bis(β -

aminoethyl ether)-*N,N,N',N'*-tetraacetic acid (#E3889; Sigma) and 25 mmol/L HEPES (#H3375; Sigma) at 37.5°C for 15 minutes. Then, the buffer was replaced with a solution containing 5 mg/mL collagenase IV (#17104019; Gibco), 4 mmol/L CaCl₂, and 0.8 mmol/L MgSO₄ for 15 minutes at a flow rate of 10 mL/min. After a few minutes of perfusion, the livers were removed rapidly, and the digested hepatic cells were dispersed into cold DMEM, calciumfree. The cell suspension generated was filtered through a sterile 70- μ m pore size nylon cell strainer (#CLS431751; Sigma) and spun 3 times at 30 \times *g* for 4 minutes. The pellets were suspended in DMEM containing 15% fetal bovine serum and 1% penicillin/streptomycin for primary hepatocyte culture.

After 24 hours of attachment, the cells were cultured with *t*BHP (#458139, 50 μ mol/L; Sigma-Aldrich) for 24 hours to mimic a state of oxidative stress model, and then cells were treated with various drugs. PAL (10, 20, and 40 nmol/L), ZVAD-FMK (#HY-16658B, 10 μ mol/L; MCE, Taiwan, ROC), necroptosis inhibitor (Necrostatin-1, #HY-15760, 10 μ mol/L; MCE), NOX1 inhibitor (apocynin, #HY-N0088, 10 μ mol/L; MCE), autophagy inhibitor (chloroquine, #HY-17589A, 10 μ mol/L; MCE), p38MAPK inhibitor (SB202190, #HY-10295, 10 μ mol/L; MCE), MAPK and MEK/ERK activator (C16-PAF, #HY-108635, 1 μ mol/L; MCE), or ROS inhibitor (N-acetyl-L-cysteine, NAC, #HY-B0215, 5 μ mol/L; MCE) were dissolved in dimethyl sulfoxide at a concentration of 10 mmol/L and stored in a dark-colored bottle at -20°C. The stock was diluted to the required concentration with dimethyl sulfoxide when needed. Cells grown in a medium containing an equivalent amount of dimethyl sulfoxide without drugs served as a control.

Plasmid Construction and Gene Transfection

Vdr shRNA, control shRNA, *Vdr* plasmid, control vector, *Atg5* siRNA, and control siRNA were ordered from Shanghai GeneChem Co, Ltd (Shanghai, China). The vectors were dissolved in serum-free DMEM. Before infection, a primary hepatocyte isolated from a wild-type C57BL/6 mouse and HepG2 cell were treated with 5 μ g/mL polybrene (#TR-1003; Sigma-Aldrich) for 4 hours. After 24 hours, cells were incubated with fresh DMEM supplemented with insulin transferrin selenium (#I3146; Sigma-Aldrich), BSA (#30063572, 4 mg/mL; Gibco), and sodium pyruvate (#S8636; Sigma-Aldrich) for 24 hours. Subsequent Western blot was performed to analyze transfection efficiency.

Cell Viability Assay

Cell viability was evaluated with a CCK8 Cell Counting Kit (#C0042; Beyotime Institute of Biotechnology) according to the manufacturer's instructions. Briefly, hepatocytes were seeded in a 96-well plate and exposed to *t*BHP (50 μ mol/L) for the indicated times. The 10 μ L CCK8 reagents were added to each well and incubated at 37°C in 5% CO₂ for 4 hours, and then the plates were measured at 450 nm using the Tecan Safire2 Multi-detection Microplate Reader (Morrisville, NC).

TUNEL Staining

Cell apoptosis was assessed using a TUNEL kit (#KGA7062; KeyGEN BioTECH, Nanjing, China). The assessment was performed as recommended by the manufacturer, and fluorescent images were finally obtained by an Olympus fluorescence microscope (DP730).

MMP Analysis

The MMP was measured using Rho123 retention in hepatocytes isolated from sham and BDL mouse liver. Hepatocytes were collected in centrifuge tubes and incubated with Rho123 (#R302, 0.5 mmol/L; Invitrogen, Waltham, MA) for 20 minutes at room temperature in the dark. After being washed with PBS, the cells were resuspended in 800 mL PBS (pH 7.4) and analyzed using flow cytometry (cytoFlex S; Beckman Coulter, Inc, Brea, CA) with excitation and emission wavelengths of 488 and 530 nm, respectively.

Quantitative Polymerase Chain Reaction Analysis

Total RNA was extracted from primary hepatocytes isolated from sham and BDL mice liver or wild-type C57BL/6 mice liver and HepG2 cell by homogenization in TRIzol reagent (#15596018; Thermo Fisher Scientific, Waltham, MA). Complementary DNA was synthesized by Revert Aid reverse transcriptase (#K1691; Thermo Fisher Scientific). Real-time polymerase chain reaction (PCR) was performed on a Bio-Rad CFX384 real-time PCR detection system using iTaq Universal SYBR Green Super mix (#1725125; Bio-Rad Laboratories, Shanghai, China). The following genes were probed with quantitative PCR using the β -actin gene as loading control: *Vdr*, *Cyp24a1*, and *Sult2a1*. Primer sequences were as follows: *Vdr*: 5'-GCCGCCTGTCTGTGTTATTC-3' (sense), 5'-GGTCATCTTGGCAGTGAGTG-3' (antisense); *Sult2a1*: 5'-AGGAACGAAGTGGCTGATTG-3' (sense), 5'-ATGGGAA-GATGGGAGGTCAT-3' (antisense); and *Cyp24a1*: 5'-CTGCCCCATTGA-CAAAAGGC-3' (sense), 5'-CTCACCGTCGGT-CATCAGC-3' (antisense). β -actin was used as a reference gene. Results are reported as normalized and calibrated ratios calculated using the 2^{- $\Delta\Delta$ CT} method.

Western Blot Analysis and Immunoprecipitation

The primary hepatocyte isolated from sham and BDL mice liver tissue or wild-type C57BL/6 mice and HepG2 cell was extracted using RIPA Lysis and Extraction Buffer (#89901; Thermo Fisher Scientific), and the protein concentration was determined by bicinchoninic acid (BCA). Samples containing equal amounts of protein (15–20 μ g) were separated by 8%–12% sodium dodecyl sulfate–polyacrylamide gel electrophoresis and transferred to polyvinylidene difluoride membranes. Membranes were blocked with 5% BSA for 2 hours at room temperature and incubated overnight at 4°C with primary antibodies against VDR (#MA1-710, 1:1000; Thermo Scientific), cleaved-caspase 3 (#9661, 1:1000; CST, Boston, MA), cleaved-caspase 8 (#8592, 1:1000; CST), cleaved-caspase 9 (#7237, 1:1000; CST), Bax (#5023, 1:1000;

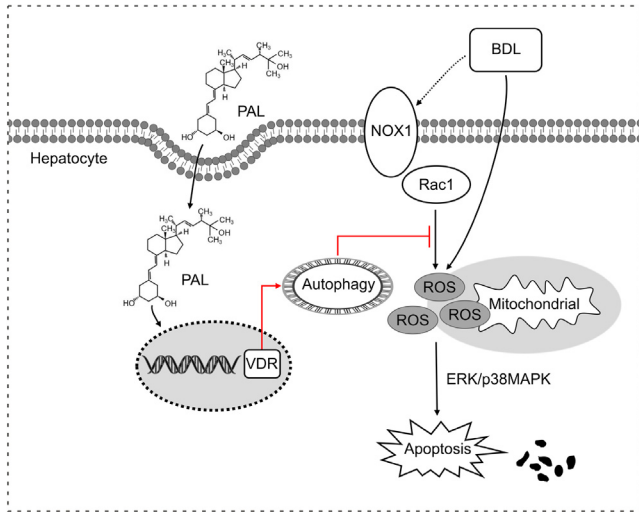


Figure 8. Proposed mechanism. In the liver, BDL led to ROS accumulation, which in turn induced hepatocyte apoptosis, resulting in cholestatic liver injury. In this schema, PAL up-regulated VDR expression, induced autophagy, inhibited ROS generation, and activated the ROS-dependent ERK/p38MAPK pathway.

CST), Bcl-2 (#15071, 1:1000; CST), cytochrome c (#11940, 1:1000; CST), glyceraldehyde-3-phosphate dehydrogenase (#60004-1-Ig, 1:2000; Proteintech, Rosemont, IL), Rac1 (#24072-1-AP, 1:1000; Proteintech), NOX1 (#ab131088, 1:1000; Abcam), Ogg1 (#15125-1-AP, 1:1000; Proteintech), LC3 (#14600-1-AP, 1:1000; Proteintech), Atg5 (#10181-1-AP, 1:1000; Proteintech), Beclin-1 (#11306-1-AP, 1:1000; Proteintech), SQSTM1/p62 (#18420-1-AP, 1:1000; Proteintech), ERK1/2 (#46951, 1:1000; CST), phospho-ERK1/2 (#4370, 1:1000; CST), p38MAPK (#8690, 1:1000; CST), and phospho-p38MAPK (#4511, 1:1000; CST). Secondary horseradish-peroxidase-conjugated anti-rabbit (#ab6721, 1:2000; Abcam) or anti-mouse antibody (#ab6728, 1:2000; Abcam) was applied. Enhanced chemiluminescence (#1705060; Bio-Rad, Hercules, CA) was used to visualize bands, which were quantified by ImageJ 5.0 software (National Institutes of Health, Bethesda, MD).

Statistical Analyses

All experiments and analyses were conducted with the experimenter blinded to the drug treatment and were performed in triplicate. All data in this study were expressed as means \pm SEM. Significant differences were determined by *t* test or 1-way analysis of variance. All statistical analyses were performed using GraphPad Prism software (version 6.0; GraphPad Software, San Diego, CA). $P < .05$ was considered significant throughout this study.

References

1. Khatun M, Ray RB. Mechanisms underlying hepatitis C virus-associated hepatic fibrosis. *Cells* 2019;8:1249.

2. Lackner C, Tiniakos D. Fibrosis and alcohol-related liver disease. *J Hepatol* 2019;70:294–304.
3. Kim S, Han SY, Yu KS, Han D, Ahn HJ, Jo JE, Kim JH, Shin J, Park HW. Impaired autophagy promotes bile acid-induced hepatic injury and accumulation of ubiquitinated proteins. *Biochem Biophys Res Commun* 2018; 495:1541–1547.
4. Santamaría E, Rodríguez-Ortigosa CM, Uriarte I, Latasa MU, Urtasun R, Alvarez-Sola G, Bárcena-Varela M, Colyn L, Arcelus S, Jiménez M, Deutschmann K, Peleteiro-Vigil A, Gómez-Cambronero J, Milkiewicz M, Milkiewicz P, Sangro B, Keitel V, Monte MJ, Marin JGG, Fernández-Barrena MG, Ávila MA, Berasain C. The epidermal growth factor receptor ligand amphiregulin protects from cholestatic liver injury and regulates bile acids synthesis. *Hepatology* 2019;69:1632–1647.
5. Panzitt K, Jungwirth E, Krones E, Lee JM, Pollheimer M, Thallinger GG, Kolb-Lenz D, Xiao R, Thorell A, Trauner M, Fickert P, Marschall HU, Moore DD, Wagner M. FXR-dependent Rubicon induction impairs autophagy in models of human cholestasis. *J Hepatol* 2020;72:1122–1131.
6. Gonzalez-Sanchez E, Firrincieli D, Housset C, Chignard N. Nuclear receptors in acute and chronic cholestasis. *Dig Dis* 2015;33:357–366.
7. Schmidt DR, Holmstrom SR, Fon Tacer K, Bookout AL, Kliewer SA, Mangelsdorf DJ. Regulation of bile acid synthesis by fat-soluble vitamins A and D. *J Biol Chem* 2010;285:14486–14494.
8. Firrincieli D, Zúñiga S, Rey C, Wendum D, Lasnier E, Rainteau D, Braescu T, Falguières T, Boissan M, Cadoret A, Housset C, Chignard N. Vitamin D nuclear receptor deficiency promotes cholestatic liver injury by disruption of biliary epithelial cell junctions in mice. *Hepatology* 2013;58:1401–1412.
9. Xie J, Fan Y, Jia R, Yang F, Ma L, Li L. Yes-associated protein regulates the hepatoprotective effect of vitamin D receptor activation through promoting adaptive bile duct remodeling in cholestatic mice. *J Pathol* 2021; 255:95–106.
10. Huang D, Guo Y, Li X, Pan M, Liu J, Zhang W, Mai K. Vitamin D(3)/VDR inhibits inflammation through NF- κ B pathway accompanied by resisting apoptosis and inducing autophagy in abalone *Haliotis discus hannai*. *Cell Biol Toxicol* 2021, Epub ahead of print.
11. Yao T, Ying X, Zhao Y, Yuan A, He Q, Tong H, Ding S, Liu J, Peng X, Gao E, Pu J, He B. Vitamin D receptor activation protects against myocardial reperfusion injury through inhibition of apoptosis and modulation of autophagy. *Antioxid Redox Signal* 2015;22:633–650.
12. Li D, Pei X, Qin X, Liu X, Li C, Li L, Dai C, Xiao X, Tang S. Olaquinox-induced liver damage involved the crosstalk of oxidative stress and p53 in vivo and in vitro. *Oxid Med Cell Longev* 2020;2020:8835207.
13. Chang SN, Kim SH, Dey DK, Park SM, Nasif O, Bajpai VK, Kang SC, Lee J, Park JG. 5-O-Demethylno-biletin alleviates ccl(4)-induced acute liver injury by equilibrating ROS-mediated apoptosis and autophagy induction. *Int J Mol Sci* 2021;22:1083.

14. Basak D, Uddin MN, Hancock J. The role of oxidative stress and its counteractive utility in colorectal cancer (CRC). *Cancers* 2020;12:3336.
15. Kabirifar R, Ghosh ZA, Safari F, Karimollah A, Moradi A, Eskandari-Nasab E. Quercetin protects liver injury induced by bile duct ligation via attenuation of Rac1 and NADPH oxidase1 expression in rats. *Hepatobiliary Pancreat Dis Int* 2017;16:88–95.
16. Chen CY, Chen KC, Yang TY, Liu HC, Hsu SL. Gallic acid induces a reactive oxygen species-provoked c-Jun N-terminal kinase-dependent apoptosis in lung fibroblasts. *Evid Based Complement Alternat Med* 2013;2013:613950.
17. Kim KY, Park KI, Kim SH, Yu SN, Park SG, Kim YW, Seo YK, Ma JY, Ahn SC. Inhibition of autophagy promotes salinomycin-induced apoptosis via reactive oxygen species-mediated PI3K/AKT/mTOR and ERK/p38 MAPK-dependent signaling in human prostate cancer cells. *Int J Mol Sci* 2017;18:1088.
18. Xiang D, Yang J, Xu Y, Lan L, Li G, Zhang C, Liu D. Estrogen cholestasis induces gut and liver injury in rats involving in activating PI3K/Akt and MAPK signaling pathways. *Life Sci* 2021;276:119367.
19. Hsu JH, Wu JR, Liou SF, Chen HM, Dai ZK, Chen IJ, Yeh JL. Labeledipinedilol-A prevents lysophosphatidylcholine-induced vascular smooth muscle cell death through reducing reactive oxygen species production and anti-apoptosis. *Atherosclerosis* 2011;217:379–386.
20. Wang Y, Deb DK, Zhang Z, Sun T, Liu W, Yoon D, Kong J, Chen Y, Chang A, Li YC. Vitamin D receptor signaling in podocytes protects against diabetic nephropathy. *J Am Soc Nephrol* 2012;23:1977–1986.
21. Chen C, Luo Y, Su Y, Teng L. The vitamin D receptor (VDR) protects pancreatic beta cells against Forkhead box class O1 (FOXO1)-induced mitochondrial dysfunction and cell apoptosis. *Biomed Pharmacother* 2019;117:109170.
22. Moradi A, Maroofi A, Hemati M, Hashemzade T, Alborzi N, Safari F. Inhibition of GTPase Rac1 expression by vitamin D mitigates pressure overload-induced cardiac hypertrophy. *Int J Cardiol Heart Vasc* 2021;37:100922.
23. Dong B, Zhou Y, Wang W, Scott J, Kim K, Sun Z, Guo Q, Lu Y, Gonzales NM, Wu H, Hartig SM, York RB, Yang F, Moore DD. Vitamin D receptor activation in liver macrophages ameliorates hepatic inflammation, steatosis, and insulin resistance in mice. *Hepatology* 2020;71:1559–1574.
24. Jia R, Yang F, Yan P, Ma L, Yang L, Li L. Paricalcitol inhibits oxidative stress-induced cell senescence of the bile duct epithelium dependent on modulating Sirt1 pathway in cholestatic mice. *Free Radic Biol Med* 2021;169:158–168.
25. Ibrahim S, Dayoub R, Krautbauer S, Liebisch G, Wege AK, Melter M, Weiss TS. Bile acid-induced apoptosis and bile acid synthesis are reduced by overexpression of augments of liver regeneration (ALR) in a STAT3-dependent mechanism. *Exp Cell Res* 2019;374:189–197.
26. Heidari R, Ghanbarinejad V, Mohammadi H, Ahmadi A, Ommati MM, Abdoli N, Aghaei F, Esfandiari A, Azarpira N, Niknahad H. Mitochondria protection as a mechanism underlying the hepatoprotective effects of glycine in cholestatic mice. *Biomed Pharmacother* 2018;97:1086–1095.
27. Guo L, Gong H, Tang TL, Zhang BK, Zhang LY, Yan M. Crizotinib and sunitinib induce hepatotoxicity and mitochondrial apoptosis in L02 cells via ROS and Nrf2 signaling pathway. *Front Pharmacol* 2021;12:620934.
28. Jun JI, Lau LF. The matricellular protein CCN1 induces fibroblast senescence and restricts fibrosis in cutaneous wound healing. *Nat Cell Biol* 2010;12:676–685.
29. Soria LR, Gurung S, De Sabbata G, Perocheau DP, De Angelis A, Bruno G, Polishchuk E, Paris D, Cuomo P, Motta A, Orford M, Khalil Y, Eaton S, Mills PB, Waddington SN, Settembre C, Muro AF, Baruteau J, Brunetti-Pierri N. Beclin-1-mediated activation of autophagy improves proximal and distal urea cycle disorders. *EMBO Mol Med* 2021;13:e13158.
30. Sheng Y, Song Y, Li Z, Wang Y, Lin H, Cheng H, Zhou R. RAB37 interacts directly with ATG5 and promotes autophagosome formation via regulating ATG5-12-16 complex assembly. *Cell Death Differ* 2018;25:918–934.
31. Klionsky DJ, Abdelmohsen K, Abe A, et al. Guidelines for the use and interpretation of assays for monitoring autophagy (3rd edition). *Autophagy* 2016;12:1–222.
32. Wang R, Hu W. Asprosin promotes β -cell apoptosis by inhibiting the autophagy of β -cell via AMPK-mTOR pathway. *J Cell Physiol* 2021;236:215–221.
33. Wu YM, Chen ZJ, Jiang GM, Zhang KS, Liu Q, Liang SW, Zhou Y, Huang HB, Du J, Wang HS. Inverse agonist of estrogen-related receptor α suppresses the growth of triple negative breast cancer cells through ROS generation and interaction with multiple cell signaling pathways. *Oncotarget* 2016;7:12568–12581.
34. Song SB, Hwang ES. High levels of ROS impair lysosomal acidity and autophagy flux in glucose-deprived fibroblasts by activating atm and ERK pathways. *Biomolecules* 2020;10:761.
35. Ma L, Ma Y, Zhang Z, Wang Q, Liu X. The signaling axis of Rac1-TFEB regulates autophagy and tumorigenesis. *Anticancer Drugs* 2019;30:1031–1037.
36. Agmon-Levin N, Kopilov R, Selmi C, Nussinovitch U, Sánchez-Castañón M, López-Hoyos M, Amital H, Kivity S, Gershwin EM, Shoenfeld Y. Vitamin D in primary biliary cirrhosis, a plausible marker of advanced disease. *Immunol Res* 2015;61:141–146.
37. Smyk DS, Orfanidou T, Invernizzi P, Bogdanos DP, Lenzi M. Vitamin D in autoimmune liver disease. *Clin Res Hepatol Gastroenterol* 2013;37:535–545.
38. Bakke D, Sun J. Ancient nuclear receptor VDR with new functions: microbiome and inflammation. *Inflamm Bowel Dis* 2018;24:1149–1154.
39. Lu W, Li X, Liu N, Zhang Y, Li Y, Pan Y, Yang J, Liu Z, Kong J. Vitamin D alleviates liver fibrosis by inhibiting histidine-rich calcium binding protein (HRC). *Chem Biol Interact* 2021;334:109355.

40. Ni HM, Bockus A, Boggess N, Jaeschke H, Ding WX. Activation of autophagy protects against acetaminophen-induced hepatotoxicity. *Hepatology* 2012;55:222–232.
41. Wang Y, Nartiss Y, Steipe B, McQuibban GA, Kim PK. ROS-induced mitochondrial depolarization initiates PARK2/PARKIN-dependent mitochondrial degradation by autophagy. *Autophagy* 2012;8:1462–1476.
42. Luo S, Rubinsztein DC. Apoptosis blocks Beclin 1-dependent autophagosome synthesis: an effect rescued by Bcl-xL. *Cell Death Differ* 2010;17:268–277.
43. Pyo JO, Jang MH, Kwon YK, Lee HJ, Jun JI, Woo HN, Cho DH, Choi B, Lee H, Kim JH, Mizushima N, Oshumi Y, Jung YK. Essential roles of Atg5 and FADD in autophagic cell death: dissection of autophagic cell death into vacuole formation and cell death. *J Biol Chem* 2005;280:20722–20729.
44. Song S, Tan J, Miao Y, Li M, Zhang Q. Crosstalk of autophagy and apoptosis: involvement of the dual role of autophagy under ER stress. *J Cell Physiol* 2017;232:2977–2984.
45. Du J, Jiang S, Hu Z, Tang S, Sun Y, He J, Li Z, Yi B, Wang J, Zhang H, Li YC. Vitamin D receptor activation protects against lipopolysaccharide-induced acute kidney injury through suppression of tubular cell apoptosis. *Am J Physiol Renal Physiol* 2019;316:1068–1077.
46. Zhu T, Liu TJ, Shi YY, Zhao Q. Vitamin D/VDR signaling pathway ameliorates 2,4,6-trinitrobenzene sulfonic acid-induced colitis by inhibiting intestinal epithelial apoptosis. *Int J Mol Med* 2015;35:1213–1218.
47. Kumar S, Nanduri R, Bhagyaraj E, Kalra R, Ahuja N, Chacko AP, Tiwari D, Sethi K, Saini A, Chandra V, Jain M, Gupta S, Bhatt D, Gupta P. Vitamin D3-VDR-PTPN6 axis mediated autophagy contributes to the inhibition of macrophage foam cell formation. *Autophagy* 2021;17:2273–2289.
48. Lu R, Zhang YG, Xia Y, Sun J. Imbalance of autophagy and apoptosis in intestinal epithelium lacking the vitamin D receptor. *FASEB J* 2019;33:11845–11856.
49. Kongara S, Karantza V. The interplay between autophagy and ROS in tumorigenesis. *Front Oncol* 2012;2:171.
50. Wang S, Sun X, Jiang L, Liu X, Chen M, Yao X, Sun Q, Yang G. 6-Gingerol induces autophagy to protect HUVECs survival from apoptosis. *Chem Biol Interact* 2016;256:249–256.
51. Gu C, Li L, Huang Y, Qian D, Liu W, Zhang C, Luo Y, Zhou Z, Kong F, Zhao X, Liu H, Gao P, Chen J, Yin G. Salidroside ameliorates mitochondria-dependent neuronal apoptosis after spinal cord ischemia-reperfusion injury partially through inhibiting oxidative stress and promoting mitophagy. *Oxid Med Cell Longev* 2020;2020:3549704.
52. Zhang Y, Lu Y, Ji H, Li Y. Anti-inflammatory, anti-oxidative stress and novel therapeutic targets for cholestatic liver injury. *Biosci Trends* 2019;13:23–31.
53. Zhang M, Lin L, Xu C, Chai D, Peng F, Lin J. VDR agonist prevents diabetic endothelial dysfunction through inhibition of prolyl isomerase-1-mediated mitochondrial oxidative stress and inflammation. *Oxid Med Cell Longev* 2018;2018:1714896.
54. Choi DH, Cristóvão AC, Guhathakurta S, Lee J, Joh TH, Beal MF, Kim YS. NADPH oxidase 1-mediated oxidative stress leads to dopamine neuron death in Parkinson's disease. *Antioxid Redox Signal* 2012;16:1033–1045.
55. Ryu M, Sung CK, Im YJ, Chun C. Activation of JNK and p38 in MCF-7 cells and the in vitro anticancer activity of alnus hirsuta extract. *Molecules* 2020;25:1073.
56. Liu B, Hu D, Zhou Y, Yu Y, Shen L, Long C, Butnaru D, Timashev P, He D, Lin T, Xu T, Zhang D, Wei G. Exosomes released by human umbilical cord mesenchymal stem cells protect against renal interstitial fibrosis through ROS-mediated P38MAPK/ERK signaling pathway. *Am J Transl Res* 2020;12:4998–5014.
57. Jung HY, Oh SH, Ahn JS, Oh EJ, Kim YJ, Kim CD, Park SH, Kim YL, Cho JH. NOX1 inhibition attenuates kidney ischemia-reperfusion injury via inhibition of ROS-mediated ERK signaling. *Int J Mol Sci* 2020;21:6911.
58. Juanola O, Hassan M, Kumar P, Yilmaz B, Keller I, Simillion C, Engelmann C, Tacke F, Dufour JF, De Gottardi A, Moghadamrad S. Intestinal microbiota drives cholestasis-induced specific hepatic gene expression patterns. *Gut Microbes* 2021;13:1–20.
59. Liao Z, Zhang X, Song C, Lin W, Cheng Y, Xie Z, Chen S, Nie Y, Li A, Zhang H, Li H, Li H, Xie Q. ALV-J inhibits autophagy through the GADD45β/MEKK4/P38MAPK signaling pathway and mediates apoptosis following autophagy. *Cell Death Disease* 2020;11:684.
60. Pan H, Wang Y, Na K, Wang Y, Wang L, Li Z, Guo C, Guo D, Wang X. Autophagic flux disruption contributes to Ganoderma lucidum polysaccharide-induced apoptosis in human colorectal cancer cells via MAPK/ERK activation. *Cell Death Disease* 2019;10:456.

Received May 31, 2022. Accepted October 17, 2022.

Correspondence

Address correspondence to: Lihua Li, MD, PhD, Department of General Surgery, Affiliated Wenling First People's Hospital, Taizhou University, 21 Mingyuan Road, Taiping District, Wenling, Taizhou City, Zhejiang Province, 317500, P R China. e-mail: lilihua1018@sina.com.

CRedit Authorship Contributions

lihua li (Data curation: Lead; Funding acquisition: Lead; Project administration: Lead; Writing – original draft: Lead)
 Zhijian Zheng (Data curation: Lead; Investigation: Lead; Methodology: Lead)
 Jing xie (Data curation: Lead; Methodology: Lead)
 Liman Ma (Data curation: Lead)
 Zhiqing Hao (Methodology: Lead)
 Weiwei Zhang (Methodology: Lead)

Conflicts of interest

The authors disclose no conflicts.

Funding

This study was supported by the National Natural Science Foundation of China grant 31571184 and Taizhou Science and Technology Planning Project 21ywb78.